Supplementary Information (SI) for Dalton Transactions.
This journal is © The Royal Society of Chemistry 2025

Supporting Information

Electrochemical Formation of Methane, Ethylene, and Ethane with a Bimetallic Nickel Complex: Is CO_2 the Source of Carbon?

Kaeden Teindl,[a] Arwen Y. Cai,[a] Declan Graham,[a] Kaitlin L. Branch,[a] Rida Farhat,[a] Samikshya Sahu,[b, c] Alannah M. Hallas,[a, b, c] and Eva M. Nichols[a]*

[a]Department of Chemistry, The University of British Columbia, Vancouver, British Columbia V6T 1Z1, Canada

[b]Stewart Blusson Quantum Matter Institute, The University of British Columbia, Vancouver, BC, V6T 1Z4, Canada

[c]Department of Physics & Astronomy, The University of British Columbia, Vancouver, BC, V6T 1Z1, Canada

Table of Contents

General synthetic and physical methods: Unless otherwise noted, all manipulations were conducted at room temperature under ambient atmospheric conditions. MeCN and THF were dried using a Pure Process Technology (Nashua, NH) solvent purification system. All other reagents and solvents were purchased from commercial sources and used without further purification, unless stated otherwise. NMR spectra were recorded on Bruker spectrometers operating at the frequencies noted below. Chemical shifts for ^{1}H and ^{13}C{^{1}H} spectra are reported in ppm relative to the observed signal of residual protonated solvent. Coupling constants are reported in Hz.

General methods for electrochemistry: Non-aqueous electrochemical experiments were conducted under Ar or CO_2 in 0.1 M tetrabutylammonium hexafluorophosphate ($TBAPF_6$) electrolyte and anhydrous MeCN. $TBAPF_6$ was crystallized three times from ethanol and dried under vacuum prior to its use. To ensure no oxygen was present in the working solution, electrolyte was sparged with Ar for ~15 minutes before every electrochemistry experiment. Cyclic voltammetry (CV) and controlled-potential electrolysis (CPE) experiments were performed using a CHI620E potentiostat from CH Instruments. The working electrode for cyclic voltammetry was a 3.0 mm diameter glassy carbon disk (Bioanalytical Systems, Inc.); between every scan the electrode was polished with a water-alumina slurry (particle size = 0.05 μM) on a felt pad, rinsed with distilled water, and dried with air. The counter electrode was a platinum wire. A silver wire in a glass tube sealed with a porous Vycor tip and filled with 0.1 M $TBAPF_6$ in MeCN was used as a pseudo-reference electrode. At the end of each experiment, potentials were referenced against the ferrocene/ferrocenium (Fc/Fc^+) couple as an external standard. The scan rate for all cyclic voltammograms was 100 mV/s unless otherwise noted. CV scans were compensated for internal resistance using the on-board compensation on the CHI620E potentiostat.

Magnetometry experiments and analysis: Magnetic susceptibility as a function of temperature and magnetization as a function of magnetic field was measured for the bimetallic Ni-complex with a Quantum Design Physical Property Measurement System (PPMS) with the Vibrating Sample Magnetometry (VSM) option. Measurements were performed between a temperature range of 2 K to 300 K and with magnetic field from 0 T to 7 T. For the sample preparation, the finely ground powdered sample was compressed inside a polypropylene powder holder, which was snapped tight into a brass trough sample holder and mounted onto the PPMS for measurement.

No magnetic ordering was observed for the sample down to 2 K. In Fig. S6 (A), the observed paramagnetic magnetic susceptibility as a function of temperature from 2 K to 300 K at a magnetic field of 1 T was fitted using a modified Curie-Weiss equation. The modified Curie-Weiss equation accounts for the temperature independent contribution to susceptibility (χ_0), which likely originates from the diamagnetic contribution of the sample and/or sample holder and manifests as a minor deviation for the linear trend that is expected from the Curie-Weiss law.[1]

According to modified Curie-Weiss Law,

$$\chi_{mol} = \chi_0 + \frac{C}{T - \theta cw}$$

where χ_{mol} is the measured molar susceptibility, χ_0 is the temperature-independent contribution, C is the Curie constant, and θcw is the Curie-Weiss temperature. Fitting the inverse molar susceptibility (χ^{-1}) versus T results in $\chi_0 = -2.2351 \times 10^{-4}\ emu\ mol_{Ni}{}^{-1}\ Oe^{-1}$, $\theta cw = -6.0\ K$, and $C = 0.8408\ emu\ K\ mol_{Ni}{}^{-1}\ Oe^{-1}$.

The effective magnetic moment, μ_{eff}, can be expressed in terms of C as:
$\mu_{eff} = \sqrt{8C}$

therefore, results in $\mu_{eff} = 2.593\ \mu_B$. This experimentally observed μ_{eff} of $2.593\ \mu_B$ is comparable to the values of similar dinickel complexes bearing axial ligands.[2-7] The magnetization as a function of magnetic field is shown in Fig. S6 (B), which further verifies the classic paramagnetic behaviour of the bimetallic Ni complex and therefore points to the absence of magnetic ordering.

Synthetic Procedures:

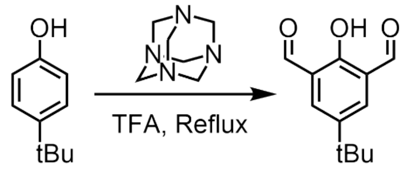

(51%)

4-*tert*-butyl-2,6-diformylphenol: This compound was synthesized according to a modified literature procedure.[8] 4-*tert*-butylphenol (3.00 g, 20 mmol) and hexamethylenetetramine (5.60 g, 40 mmol) were dissolved in trifluoroacetic acid (40 mL). The solution was then heated to 120 ^{O}C and stirred for 20 hours. After cooling to room temperature, ~150 mL of 1 M HCl was added, and the solution was stirred vigorously until a yellow precipitate formed. The precipitate was collected by vacuum filtration and washed with copious amounts of distilled water. The isolated solid was crystallized from EtOH/water and the target compound was obtained as pale-yellow crystals (2.10 g, 51% yield). ^{1}H NMR (300 MHz, DMSO) δ 11.45 (s, 1H), 10.25 (s, 2H), 8.08 (s, 2H), 1.31 (s, 9H). ESI-MS calculated for $C_{12}H_{14}O_3Na$ (M+Na)$^+$ 229.1, found 229.2.

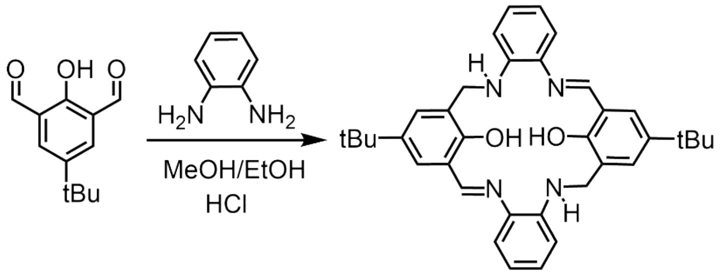

H_4L

(48%)

H_4L: This compound was synthesized according to a modified literature procedure.[9] Briefly, 4-*tert*-butyl-2,6-diformylphenol (1.00 g, 4.9 mmol) was dissolved in an ethanolic solution (90 mL) containing 170 µL of 37% HCl. A solution of 1,2-phenylenediamine (0.53 g, 4.9 mmol) dissolved in MeOH (10 mL) was then added dropwise to the ethanolic solution over the course of ~20 minutes. The reaction mixture was left to stir overnight, and a bright orange precipitate was then isolated by vacuum filtration. The precipitate was washed with a minimal amount of cold ethanol to afford **H_4L** as an orange solid (0.65 g, 48% yield). ^{1}H NMR (300 MHz, DMSO) δ 13.73 (s, 2H), 8.95 (s, 2H), 7.62 (d, J = 5.5 Hz, 4H), 7.24 (t, J = 8.5 Hz, 4H), 7.03 (d, J = 7.9 Hz, 2H), 6.76 (t, J = 7.4 Hz, 2H), 6.25 (t, J = 5.7 Hz, 2H), 4.47 (d, J = 5.4 Hz, 4H), 1.31 (s, 18H). ESI-MS calculated for $C_{36}H_{39}N_4O_2$ (M)$^-$ 559.3, found 559.3.

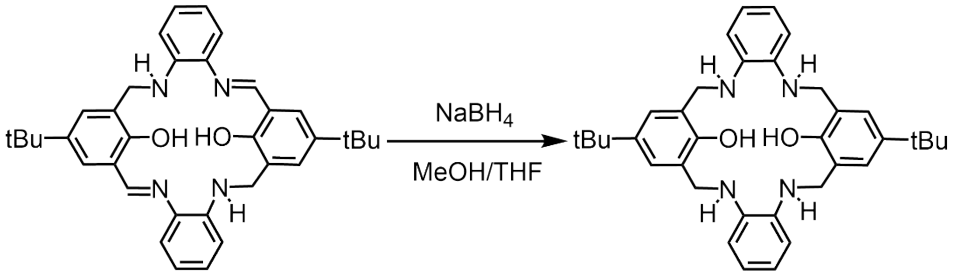

H_4L **H_6L**
(70%)

H_6L: This compound was synthesized according to a modified literature procedure.[9] **H_4L** (0.50 g, 0.90 mmol) was dissolved in a 1:1 mixture of MeOH:THF (40 mL total). $NaBH_4$ (0.40 g) was then added portion-wise over the course of ~5 minutes, and the solution turned from dark red to light yellow. The mixture was then left to stir at room temperature overnight. Subsequently, ~250 mL of distilled water was added to the solution and a pale-yellow solid was collected by vacuum filtration. The isolated solid was dissolved in DCM and this solution was filtered to remove insoluble impurities. Slow evaporation of the DCM solution afforded purified **H_6L** as pale-yellow crystals (0.35 g, 70% yield). ^1H NMR (300 MHz, DMSO) δ 9.02 (s, 2H), 7.27 (s, 4H), 6.82 – 6.58 (m, 8H), 4.86 (t, J = 5.2 Hz, 4H), 4.22 (d, J = 4.8 Hz, 8H), 1.25 (s, 18H).^{13}C NMR (75 MHz, DMSO) δ 153.40, 141.08, 136.74, 126.54, 124.14, 118.51, 110.99, 46.21, 33.68, 31.40. ESI-MS calculated for $C_{36}H_{45}N_4O_2$ $(M+H)^+$ 565.4, found 565.4.

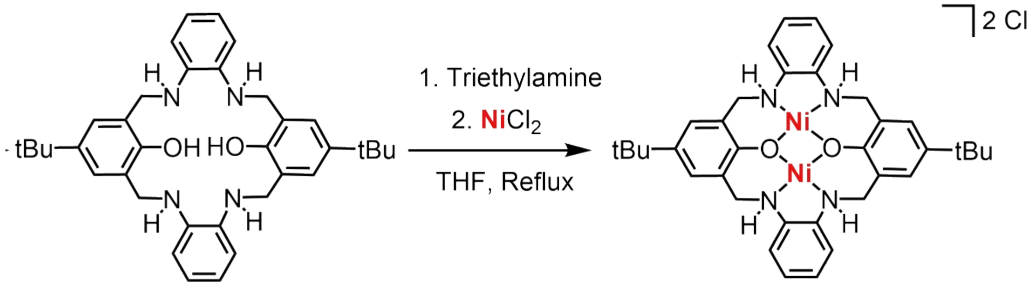

H_6L **Ni_2L**
(89%)

Ni_2L: Under an N_2 atmosphere, **H_6L** (110 mg, 0.20 mmol) and triethylamine (56 µL, 0.40 mmol) were dissolved in dry THF (40 mL), and the solution was stirred for ~10 minutes. $NiCl_2$ (52 mg, 0.40 mmol) was subsequently added, and the suspension was left to reflux under N_2 overnight. The reaction mixture was concentrated and filtered, and subsequent evaporation of the filtrate gave a dark brown oil. After vigorous stirring in dry Et_2O, a brown solid was collected by filtration. Subsequent washing with water afforded the bimetallic nickel chloride complex as a light brown powder (130 mg, 89% yield). *Note: when exposed to air for extended periods of time, the metal complex will slowly undergo spontaneous dehydrogenation to form the tetraimine complex*. HR-ESI-MS calculated for $[C_{36}H_{40}N_4O_2Ni_2Cl]^-$ (M – 2H – Cl)$^-$ 713.1519, found 713.1517. UV-Vis in MeOH [λ_{max}/nm (ε/M^{-1} cm^{-1})]: 362 (395), 420 (253), 605 (18). μ_{eff} = 2.593 per Nickel.

Spectroscopic, mass spectrometry, and magnetic characterization data:

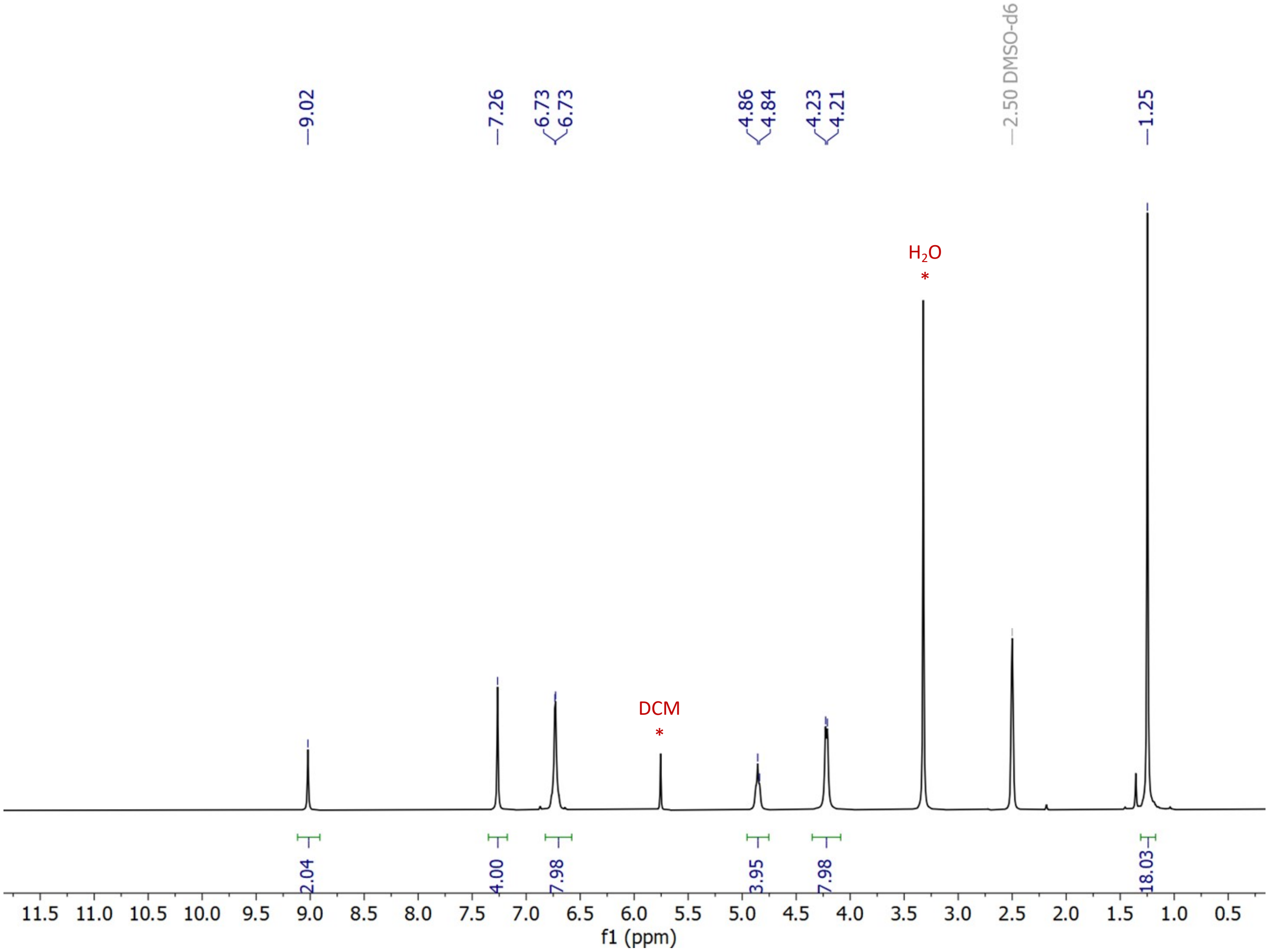

Figure S1. ^{1}H NMR of **H$_6$L** in DMSO-*d$_6$*. The signals at 3.33 and 5.76 ppm are from residual H_2O and DCM, respectively.

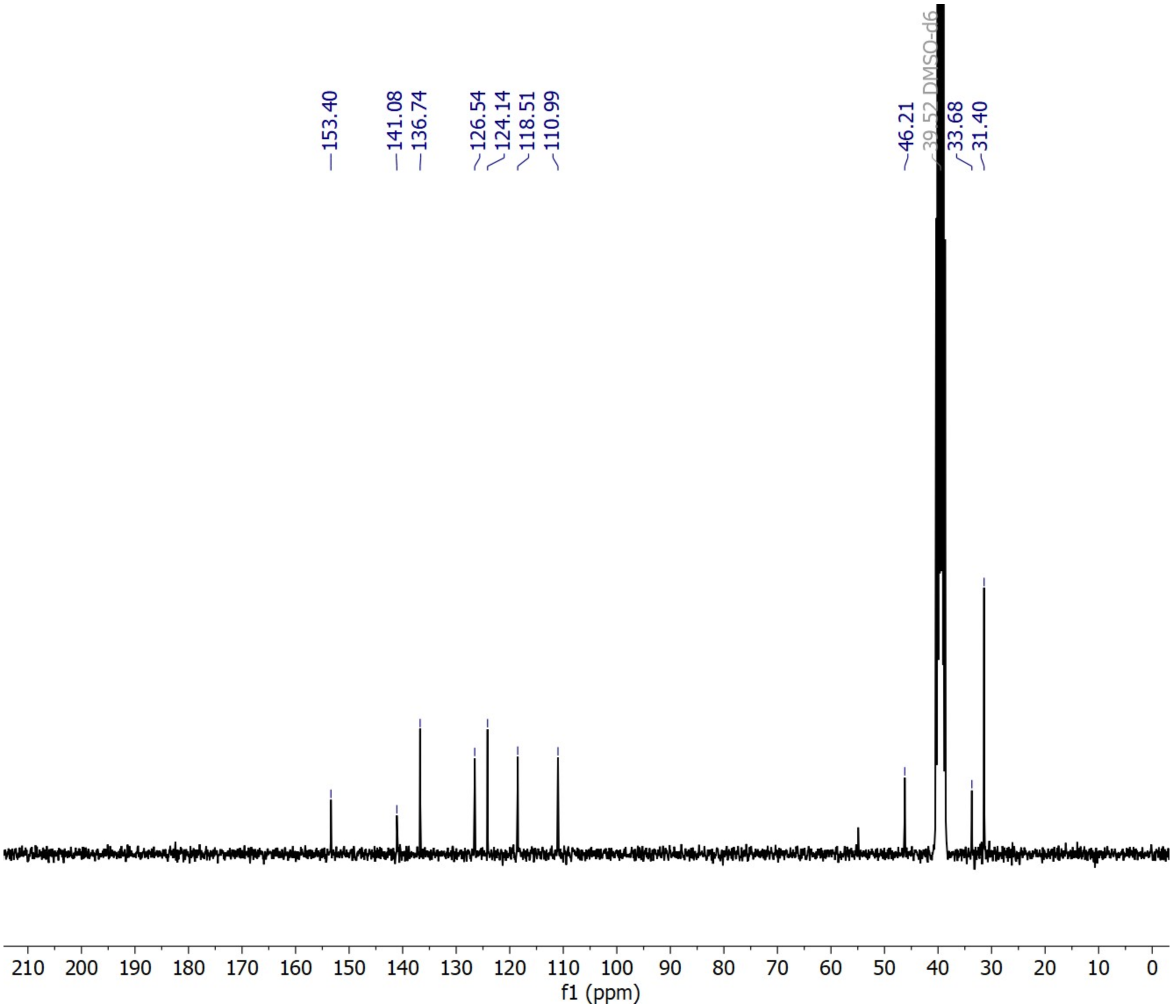

Figure S2. $^{13}C\{^1H\}$ NMR of $\mathbf{H_6L}$ in DMSO-d_6.

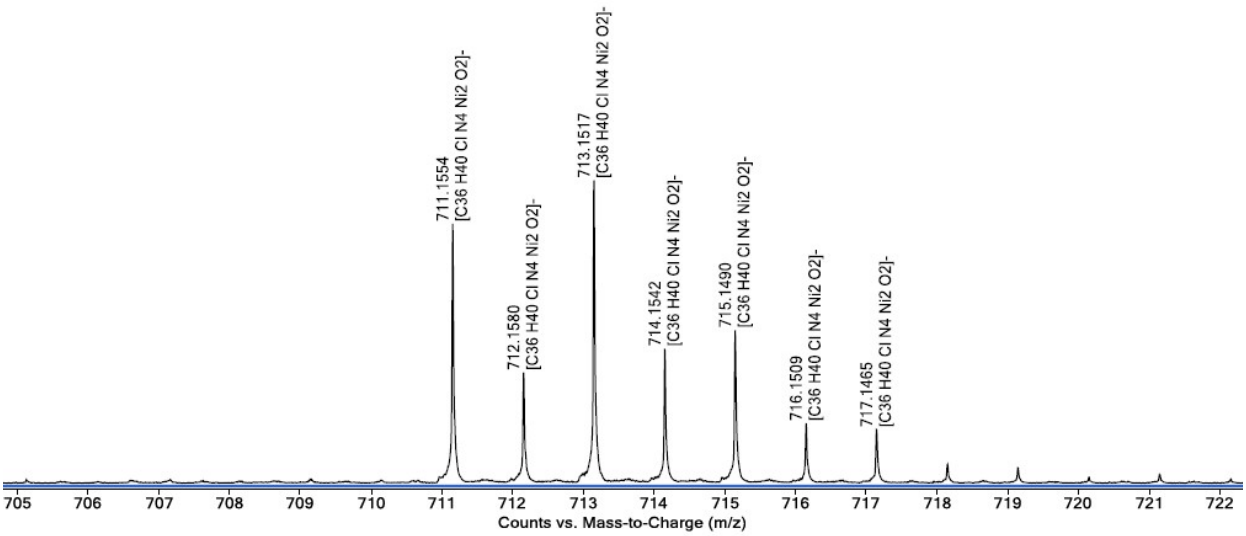

Figure S3. High resolution ESI-MS data for **Ni$_2$L** in negative ion mode.

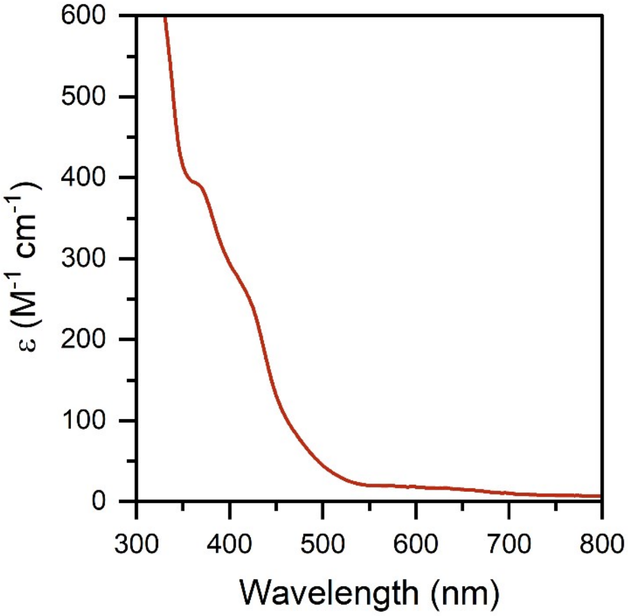

Figure S4. UV-vis spectrum of 1 mM **Ni$_2$L** in methanol.

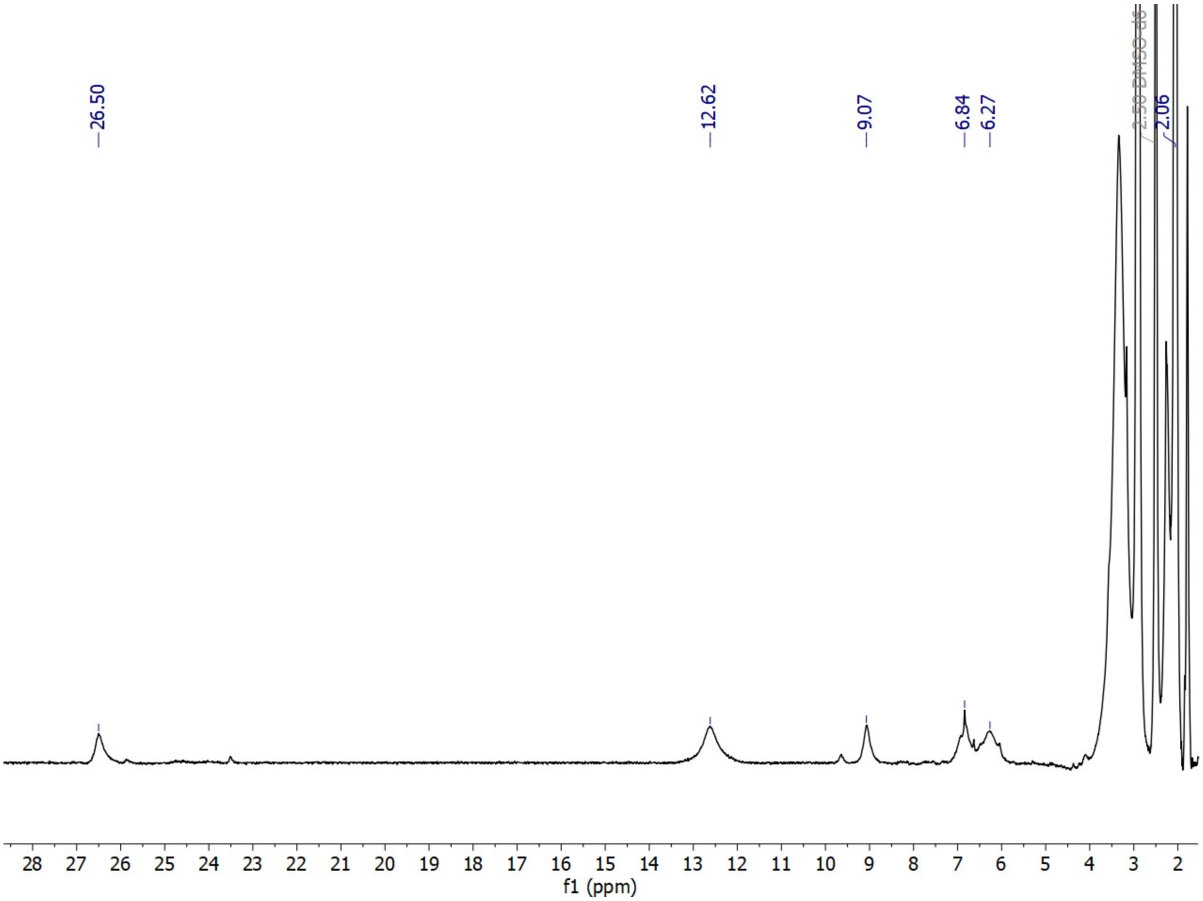

Figure S5. ^{1}H NMR of paramagnetic **Ni$_2$L** in DMSO-*d$_6$*.

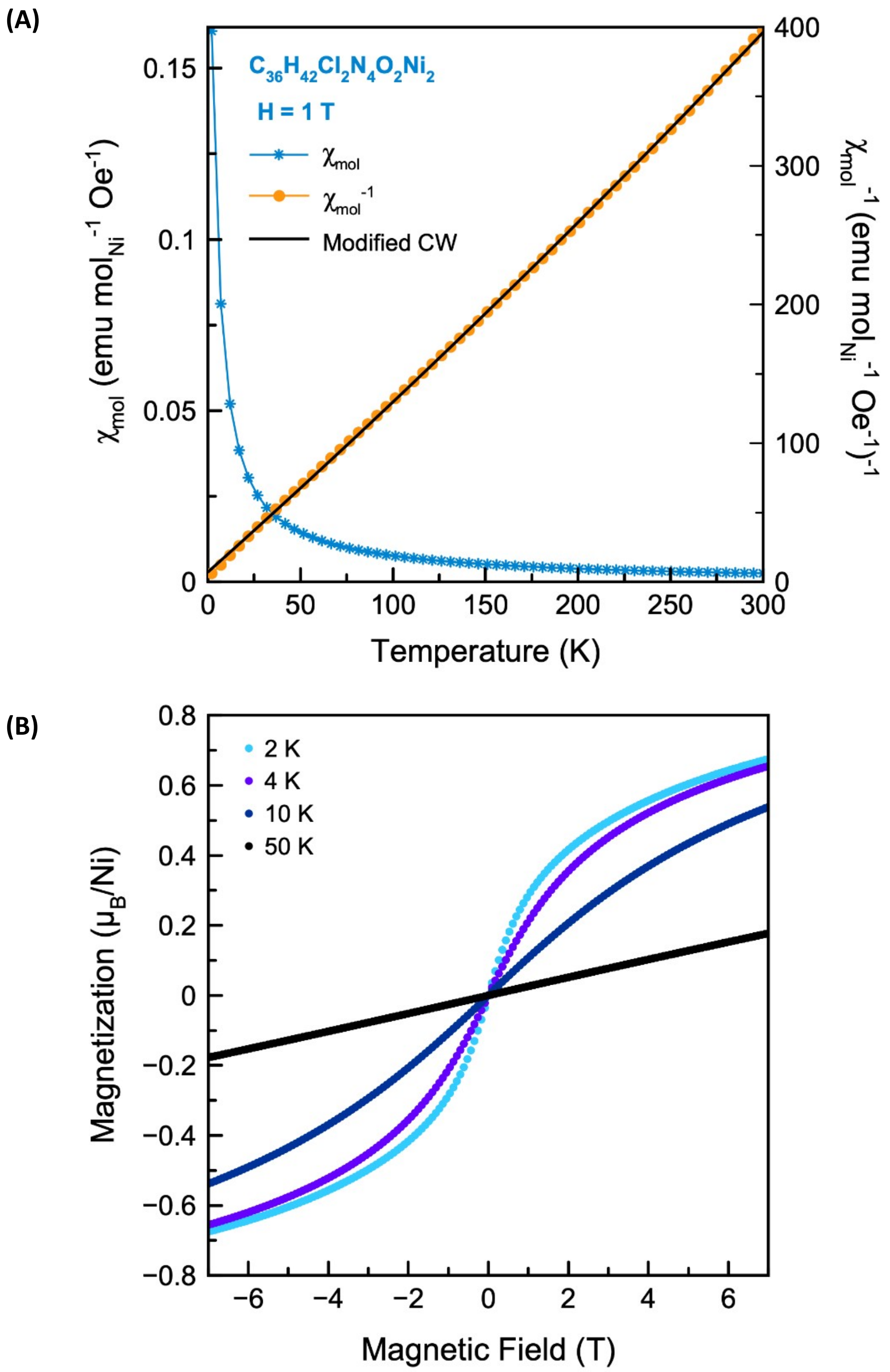

Figure S6. SQUID magnetometry of **Ni_2L**. **(A)** Magnetic susceptibility (blue) or inverse magnetic susceptibility (orange) versus temperature at 1T with modified Curie-Weiss fit (black line). The Curie-Weiss temperature is -6.0194 K, indicating antiferromagnetic coupling between the two Ni centres. **(B)** Magnetization (per Ni) versus magnetic field at 2, 4, 10, and 50 K.

Cyclic Voltammetry Data:

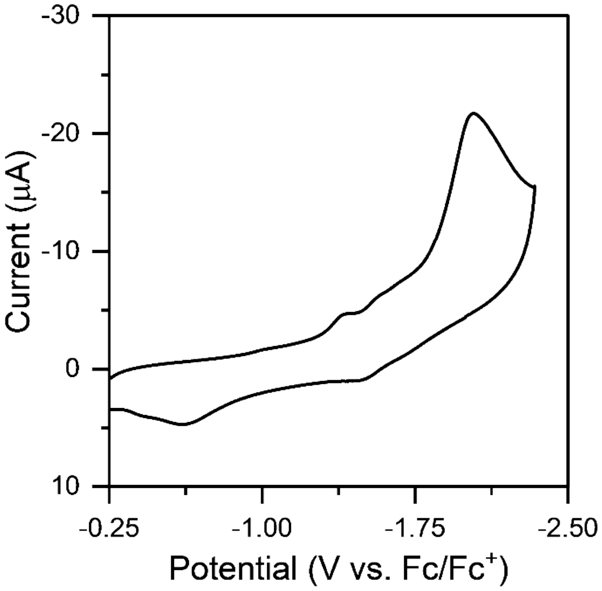

Figure S7. Cyclic voltammogram of 1 mM **Ni_2L** under 1 atm argon in dry 0.1 M $TBAPF_6$/MeCN electrolyte, scan rate = 0.1 V s^{-1}.

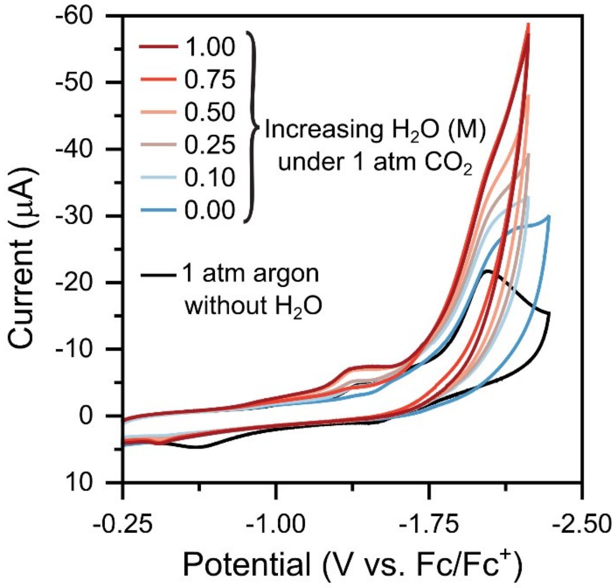

Figure S8. Cyclic voltammograms of Ni_2L under 1 atm argon (black trace) and CO_2 with increasing concentrations of water (colored traces). Conditions: 1 mM **Ni_2L,** 0.1 M $TBAPF_6$/MeCN, scan rate = 0.1 V s^{-1}.

Controlled potential electrolysis experiments: Controlled-potential electrolysis (CPE) experiments were conducted in a gas-tight PEEK electrolysis cell that we have previously reported.[10] The CPE cell has working (20 mL volume) and counter (6 mL volume) electrode compartments that are separated by a polymer separator (Daramic). The cell consists of four principal components: a working electrode compartment, lid, window covering, and counter electrode compartment. The cell contains quartz windows on the sides of both the working and counter electrode compartments.

In the working compartment, a 1 mM solution of catalyst in 7 mL of 0.1 M $TBAPF_6$/MeCN electrolyte containing exogenous water was prepared. The counter electrode compartment was filled with a 3 mL solution of 0.1 M $TBAPF_6$/MeCN. Using mass flow controllers (Alicat Scientific), the working compartment was sparged with a mixture of 95% CO_2, CO, or argon and 5% He (internal standard) for ~30 min. The cell was then sealed, and a CV was collected to determine the potential needed for the CPE experiment. The solution was then stirred at 1100 rpm with a 1 cm stir bar and the CPE experiment was commenced. At the end of each CPE experiment, the headspace was directly evacuated into the sampling loop of a gas chromatograph (SRI-GC Multiple Gas Analyzer #5) equipped with 6' Hayesep D and 13X Molecular Sieve columns, as well as a second Hayesep D guard column to trap solvent. An in-line TCD was employed for He and H_2 detection, and an FID outfitted with a methanizer was used for detection of CO, CH_4, C_2H_4, and C_2H_6. Analytes were quantified by comparing the ratio of analyte:He peak integrals to a calibration curve with known quantities of analyte (Figures S9-S11).

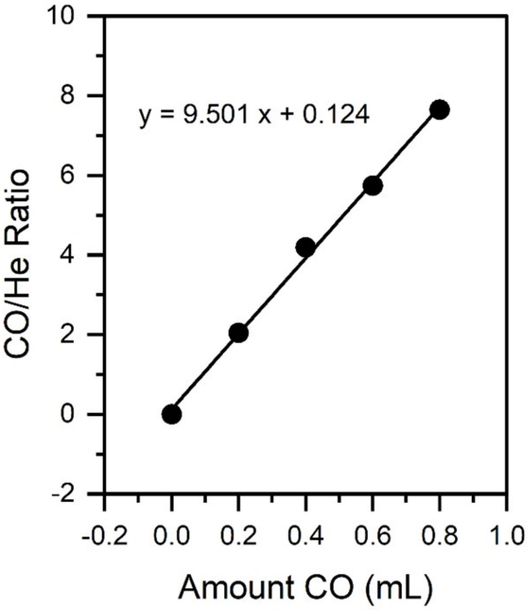

Figure S9. GC calibration curve for CO with He as the internal standard. CO/He ratio is the ratio of peak integrals measured by the FID for CO and TCD for He.

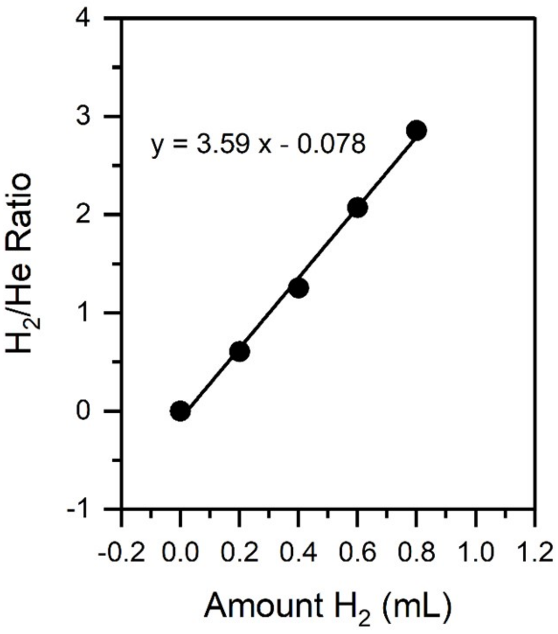

Figure S10. GC calibration curve for H_2 with He as the internal standard. H_2 /He ratio is the ratio of peak integrals measured by the TCD for H_2 and He.

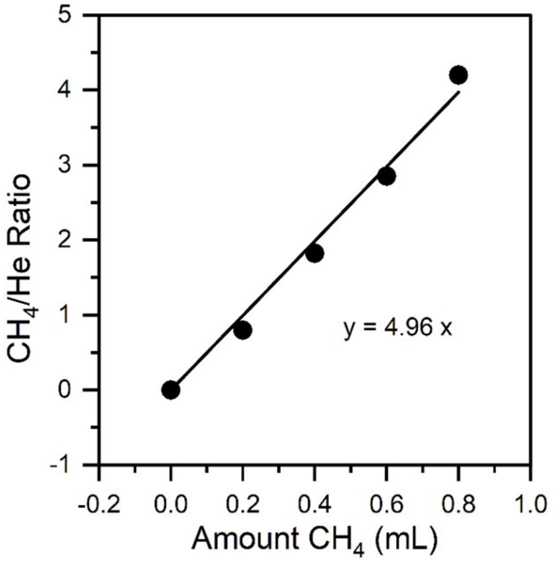

Figure S11. GC calibration curve for CH_4 with He as the internal standard. CH_4 /He ratio is the ratio of peak integrals measured by the FID for CH_4 and TCD for He.

CPE results with 1 M H_2O under 1 atm CO_2:

Potential (V vs. Fc/Fc$^+$)	Charge (C)	FE_{CH4} (%)	FE_{CO} (%)	FE_{H2} (%)
-2.4	4.90	n.d.	3	70

Table S1. Results for CPE replicates, including electrolysis potential, the charge passed (Q), and the Faradaic Efficiency (%) for gaseous products. n.d. indicates not detected.

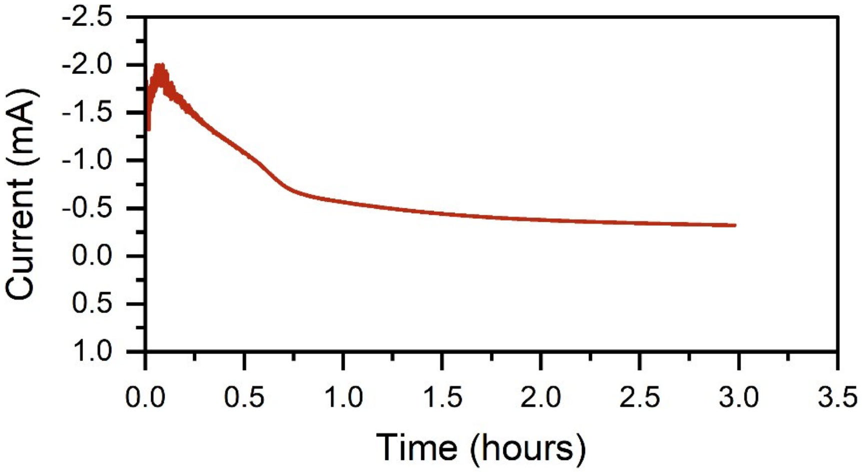

Figure S12. CPE trace of 1 mM **Ni_2L** with 1 M H_2O in 0.1 M $TBAPF_6$/MeCN under 1 atm CO_2.

CPE results with 0.25 M H_2O under 1 atm CO_2:

Potential (V vs. Fc/Fc$^+$)	Charge (C)	FE_{CH4} (%)	FE_{CO} (%)	FE_{H2} (%)
-2.3	8.12	3.8	2.5	50
-2.4	5.08	3.3	3.2	57
-2.3	8.09	3.5	2.4	53

Table S2. Results for CPE replicates, including electrolysis potential, the charge passed (Q), and the Faradaic Efficiency (%) for gaseous products.

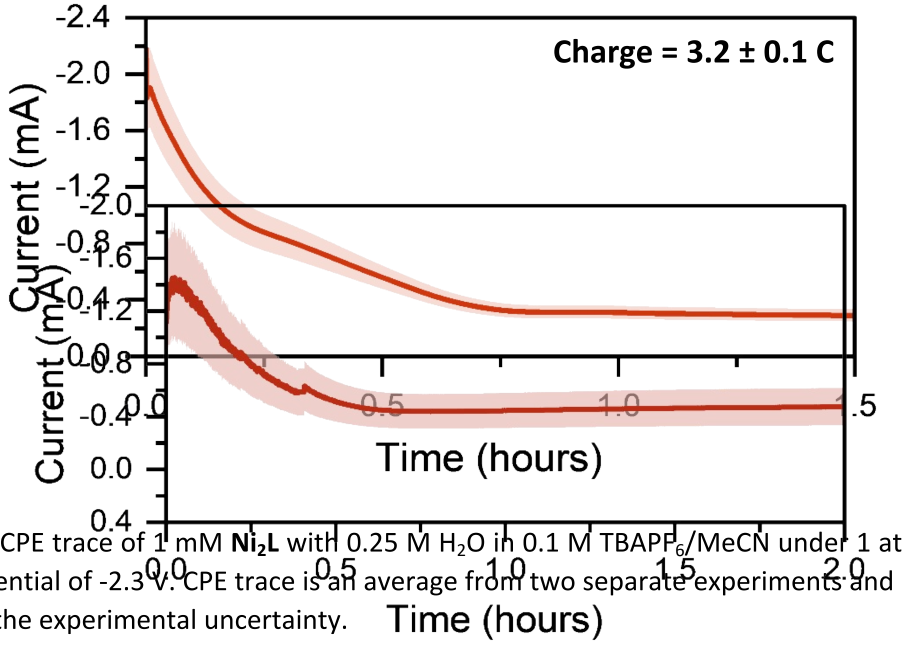

Figure S14. CPE trace of 1 mM **Ni_2L** with 0.25 M H_2O in 0.1 M $TBAPF_6$/MeCN under 1 atm argon at an applied potential of -2.3 V. CPE trace is an average from two separate experiments and shaded region represents the experimental uncertainty.

Figure S13. CPE traces of 1 mM **Ni_2L** with 0.25 M H_2O in 0.1 M $TBAPF_6$/MeCN under 1 atm CO_2. CPE results are summarized in Table S2.

CPE results with 0.25 M H_2O under 1 atm CO:

Potential (V vs. Fc/Fc^+)	Charge (C)	FE_{CH4} (%)	FE_{H2} (%)
-2.4	1.40	n.d.	n.d.

Table S3. Results for CPE experiments under 1 atm CO, including electrolysis potential and the charge passed (Q). n.d. indicates not detected.

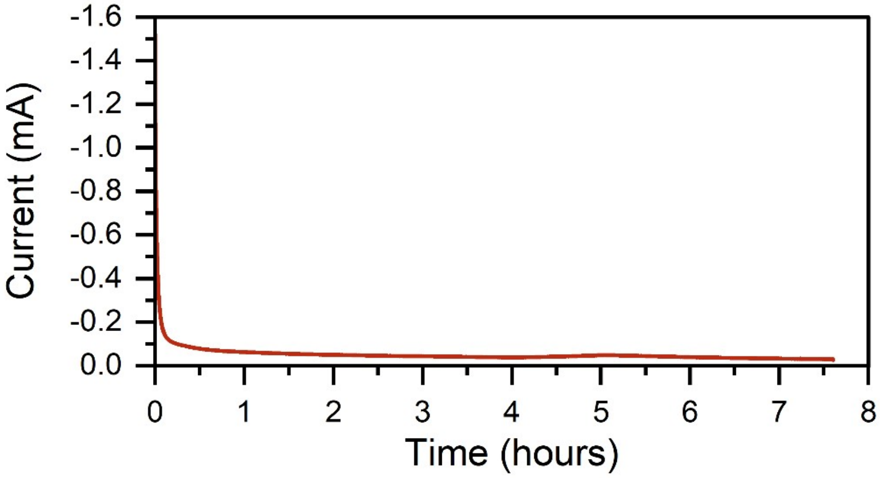

Figure S15. CPE trace of 1 mM **Ni_2L** with 0.25 M H_2O in 0.1 M $TBAPF_6$/MeCN under 1 atm CO.

Rinse test experiments: First, a CPE experiment was performed as described above (see "Controlled potential electrolysis experiments"), under a CO_2 atmosphere using 0.25 M H_2O and 1 mM catalyst. After electrolysis, the working electrode was rinsed with electrolyte (0.1 M $TBAPF_6$/MeCN) and placed in an electrolyte solution that contained 0.25 M H_2O but no catalyst. The electrolyte solution was then sparged with CO_2, and a second CPE was carried out. Similar potentials were applied in both CPE experiments.

Catalyst	Potential (V vs. Fc/Fc$^+$)	Charge (C)	FE_{CH4} (%)	FE_{CO} (%)	FE_{H2} (%)
Ni_2L (pre-rinse)	-2.3	8.12	3.8	2.5	50
Rinse Test	-2.3	0.23	n.d.	Trace	n.d.

Table S4. Results for CPE replicates from rinse test experiments, including electrolysis potential, the charge passed (Q), and the Faradaic Efficiency (%) for gaseous products. n.d. indicates product not detected.

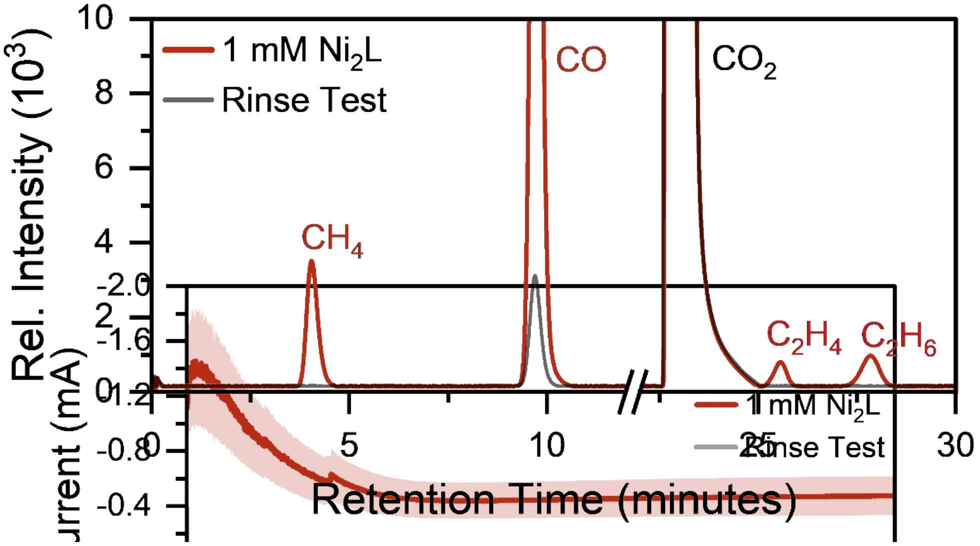

Figure S17. GC analysis of headspace gases for CPE performed under CO_2 with **Ni_2L** (red) and without **Ni_2L** during the rinse test (gray). CPE Conditions: 0.25 M H_2O, and 0.1 M $TBAPF_6$/MeCN 1 atm CO_2.

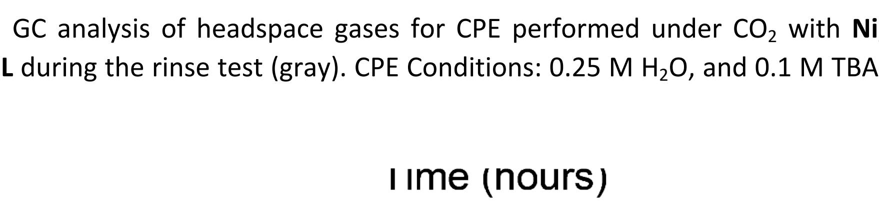

Figure S16. CPE traces of 1 mM **Ni_2L** (red) and the rinse test (grey) with 0.25 M H_2O in 0.1 M $TBAPF_6$/MeCN under 1 atm CO_2. CPE results are summarized in Table S4.

$^{13}CO_2$ labeling experiments and high-resolution MS detection of gaseous products: Inside of the CPE cell described above (see "Controlled potential electrolysis experiments"), an electrolyte solution (0.1 M $TBAPF_6$/MeCN) containing 1 mM catalyst and 0.25 M Milli-Q H_2O was sparged with N_2 for ~45 minutes. The solution was then sparged with labelled $^{13}CO_2$ (≥99 atom% ^{13}C; Sigma-Aldrich) for ~1 minute. A cyclic voltammogram was then obtained to determine the potential needed for electrolysis, and the CPE experiment was initiated (Figure S10). After electrolysis, headspace gases in the CPE cell were sampled via high-resolution GC-MS using an Agilent 7890B gas chromatograph coupled to an 5977A mass spectrometer equipped with an electron impact ion source. The instrument was run in splitless mode, the electron ionization energy was set at 70 eV, and the instrument was tuned to 10,000 resolution. In each experiment, 1 mL of headspace gas was directly injected onto the column using a gas-tight syringe. The analogous set of experiments were also performed to detect gases during the reduction of unlabelled $^{12}CO_2$. All data were calibrated according to the m/z of O^+ (*m/z* = 15.9944).

Substrate	**Potential (V vs. Fc/Fc$^+$)**	**Charge (C)**
$^{12}CO_2$	-2.4	11.01
$^{13}CO_2$	-2.4	42.50

Table S5. CPE results for labelling experiments, including electrolysis potential, the charge passed (Q).

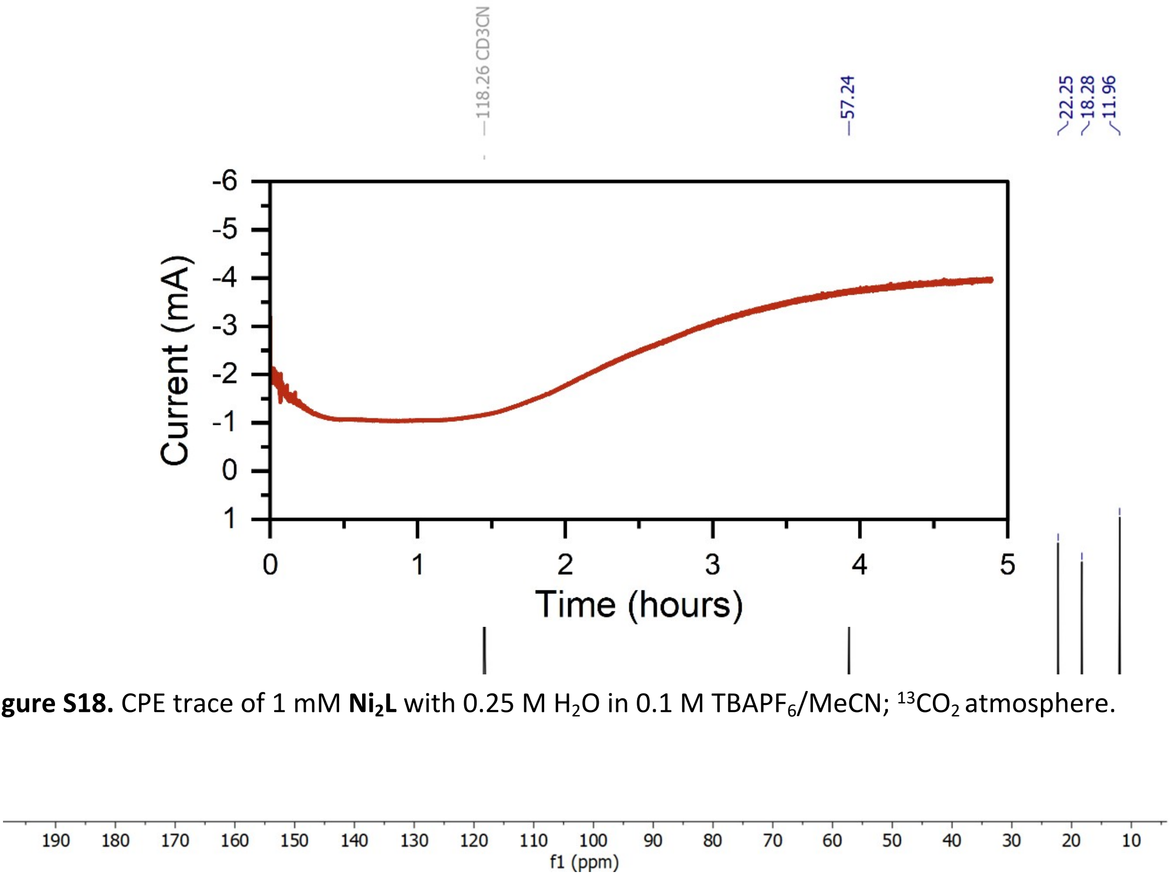

Figure S18. CPE trace of 1 mM **Ni_2L** with 0.25 M H_2O in 0.1 M $TBAPF_6$/MeCN; $^{13}CO_2$ atmosphere.

Figure S19. $^{13}C\{^1H\}$ NMR of electrolyte solution after a CPE with $^{13}CO_2$. Signal at 118.26 is from MeCN, all other signals are from residual $TBAPF_6$.

Assignment of Cationic Fragments from HR-MS data					Other Possible Cation Fragment Assignments					
Substrate	**observed mass**	**assignment**	**expected mass**	**delta**	**assignment**	**expected mass**	**delta**	**assignment**	**expected mass**	**delta**
$^{12}CO_2$	15.0231	CH_3	15.02290	0.00020	NH	15.0104	-0.0127			
	16.027	CH_4	16.03080	-0.00380	NH_2	16.0182	-0.0088			
	15.9944	O	15.9944	0.00000						
	17.0036	OH	17.0022	0.00140						
	18.0121	H_2O	18.01057	0.00153						
	28.0306	C_2H_4	28.03080	-0.00020	CH_2N	28.0182	-0.0124	CO	27.9944	-0.0362
	28.0067	N_2	28.0056	0.00110	CO	27.9944	-0.0123			
	30.0465	C_2H_6	30.0464	0.00010	CH_2O	30.01	-0.0365			
	31.9978	O_2	31.9893	0.00850						
Substrate	**observed mass**	**assignment**	**expected mass**	**delta**	**assignment**	**expected mass**	**delta**	**assignment**	**expected mass**	**delta**
$^{13}CO_2$	16.0265	$^{13}CH_3$	16.02630	0.00020	CH_4	16.03080	0.00430			
	15.9944	O	15.9944	0.00000						
	17.002	OH	17.0022	-0.00020						
	17.0337	$^{13}CH_4$	17.0341	-0.00040	NH_3	17.026	-0.0077			
	18.0097	H_2O	18.01	-0.00030						
	28.005	N_2	28.0056	-0.00060						
	28.9978	^{13}CO	28.9977	0.00010	CHO	29.0022	0.0044			
	30.034	CH_4N	30.0338	0.00020	$^{12}C^{13}CH_5$	30.04193	0.00793	$^{13}C_2H_4$	30.03746	0.00346
	31.0452	$^{13}C_2H_5$	31.0453	-0.00010	$^{12}C^{13}CH_6$	31.0498	0.0046	CH_5N	31.0417	-0.0035
	31.9897	O_2	31.9893	0.00040						

Table S6. A summary of the cationic fragments observed during HR-MS analysis and their possible assignments. The list of fragments highlighted in the pink column (left) represent the most plausible assignments. The fragments in the blue column (right) are fragments that exhibit m/z values that are similar to the observed m/z, but do not match the data as well as those fragments in the column on the left.

References:

1. S. Mugiraneza and A. M. Hallas, *Comm. Phys.*, 2022, **5**, 95.
2. C. L. Spiro, S. L. Lambert, T. J. Smith, E. N. Duesler, R. R. Gagne and D. N. Hendrickson, *Inorg. Chem.*, 1981, **20**, 1229-1237.
3. R. R. Gagne, W. A. Marritt, D. N. Marks and W. O. Siegl, *Inorg. Chem.*, 1981, **20**, 3260-3267.
4. U. Casellato, P. A. Vigato, D. E. Fenton and M. Vidali, *Chem. Soc. Rev.*, 1979, **8**, 199-220.
5. M. Tanaka, M. Kitaoka, H. Okawa and S. Kida, *Bull. Chem. Soc. Jpn.*, 1976, **49**, 2469-2473.
6. C. Fraser and B. Bosnich, *Inorg. Chem.*, 1994, **33**, 338-346.
7. L. M. Liable-Sands, C. Incarvito, A. L. Rheingold, C. J. Qin, A. L. Gavrilova and B. Bosnich, *Inorg. Chem.*, 2001, **40**, 2147-2155.
8. L. F. Lindoy, G. V. Meehan and N. Svenstrup, *Synthesis*, 1998, **7**, 1029-1032.
9. C. A. Swamy P, E. Solel, O. Reany and E. Keinan, *Chem. Eur. J.*, 2018, **24**, 15319-15328.
10. K. Teindl, B. O. Patrick and E. M. Nichols, *J. Am. Chem. Soc.*, 2023, **145**, 17176-17186.